Carbon 141 (2019) 266–273

Contents lists available at ScienceDirect

Carbon

journal homepage: www.elsevier.com/locate/carbon

Graphene as an electrochemical transfer layer

Tiva Sharifi [a, b, *, 1], Yu Xie [a, 1], Xiang Zhang [a], Hamid Reza Barzegar [b, c], Jincheng Lei [a], Gabriel Coulter [a, d], Shiyun Sun [a], Chandrasekhar Tiwary [a, e], Alex Zettl [c], Boris Yakobson [a], Pulickel M. Ajayan [a, **]

[a] Department of Materials Science and Nanoengineering, Rice University, Houston, 77005, USA
[b] Department of Physics, Umeå University, Umeå, 90187, Sweden
[c] Department of Physics, University of California, Berkeley, 94720-1234, USA
[d] School of Physics and Chemistry, Trinity College Dublin, Dublin 2, Ireland
[e] Metallurgical and Materials Engineering, Indian Institute of Technology, Kharagpur, West Bengal 721302, India

ARTICLE INFO

Article history:
Received 2 August 2018
Received in revised form
8 September 2018
Accepted 18 September 2018
Available online 20 September 2018

ABSTRACT

The capability of graphene to adopt a property from an adjacent material is investigated by measuring the electrochemical performance of a monolayer graphene placed on top of thin cobalt oxide (Co_3O_4) nanosheets. In this assembly, monolayer graphene works as an interfacial layer which inhibits the direct contact of the actual electroactive material and electrolyte during electrochemical reaction. The results show that while graphene is electrochemically inert, it behaves as an active material to catalyze oxygen evolution reaction (OER) once placed on top of Co_3O_4 nanosheets. The graphene-covered Co_3O_4 model system shows electrochemical performance similar to Co_3O_4 indicating complete transference of the electrochemical property of the metal oxide to the graphene. Based on density functional theory (DFT) calculations, charge transfer from graphene to Co_3O_4 is the key factor for turning the electrochemically inactive graphene to an apparent active material.

1. Introduction

Graphene is the most explored two dimensional (2D) material and even though its properties are well manifested, more are established continuously [1]. Electronic and thermal properties of graphene have been extensively tuned by introducing defects, guest elements and external functionalities or by engineering the grain boundaries [2–4]. It is shown that the band structure of graphene can be tuned by a nearby substrate and hence the pristine graphene (pure carbon) act as a doped graphene layer [5–7]. Recently, it is unrevealed that graphene can surprisingly perform superconductivity by introducing a "magic" angle between two adjacent graphene layers [8]. From a fundamental point of view it is fascinating to tune and expand the properties of graphene without disturbing its structure. It is even more interesting to unreveal the capability of graphene to adopt an extrinsic property from a materials which is placed in its close vicinity. As monolayer graphene demonstrates a relatively high mobility of carriers, charge transfer can be one of the best strategies to transfer certain characteristics from and to graphene [9,10]. This gives the possibility to induce several extrinsic properties and expand the functionality of this fascinating single element 2D material. Monolayer graphene is among the most chemically and electrochemically inert materials due to lack of enough edge planes and surface charges [11]. Graphene, if placed on top of an electrochemically active material, should serve as a perfect model system to demonstrate the hypothesis of transfer electrochemical property. In this model system, graphene act as an interfacial layer to avoid the direct contact of the actual electrochemically active material with electrolyte in the electrochemical test cell. In this way the performance of graphene during electrochemical reaction is solely induced from under-layer material.

Here, we demonstrate the capability of monolayer graphene to adopt a particular property of an adjacent material. We measure the electrochemical behavior of a monolayer graphene and compare it with the performance of a model system where the uniform monolayer graphene completely covers electrochemically active Co_3O_4 nanosheets in oxygen evolution reaction (OER) [12].

* Corresponding author. Department of Physics, Umeå University, Umeå, 90187, Sweden.
** Corresponding author.
E-mail addresses: tiva.sharifi@umu.se (T. Sharifi), ajayan@rice.edu (P.M. Ajayan).
[1] These authors contributed equally to the paper.

https://doi.org/10.1016/j.carbon.2018.09.056
0008-6223/

We show that while graphene itself is completely electrochemically inactive, if placed on top of Co_3O_4, adopts electrochemical capability of Co_3O_4 in such a way that both Co_3O_4 and graphene/Co_3O_4 perform similarly in catalyzing OER. It is also observed that bilayer or thicker graphene layers are unable to adopt the electrochemical performance of the under-layer material. Based on DFT calculations, carbon atoms in monolayer graphene become electron donors once positioned on top of Co_3O_4. Graphene is then act as a p-doped material which is the key factor for turning the electrochemically inactive graphene into an active material. The result of this experiment combined with comprehensive computational analysis, demonstrates not only a rout to tune and expand the properties of graphene but also the transference of electrochemical performance of the materials through graphene.

2. Experimental

2.1. Material and electrode preparation

Synthesis of Co_3O_4 nanosheet. Co_3O_4 nanosheets were synthesized with a similar method as reported before [13] with some modifications. 200 mg Pluronic® F-127 (from Sigma-Aldrich) was dissolved in 16 ml ethanol and 1 ml of water by stirring. Then 0.5 mM of cobalt acetate tetrahydrate ($Co(C_2H_3O_2)_2$-from Sigma-Aldrich) and 0.5 mM Hexamethylenetetramine (HMTA-from Sigma-Aldrich) was added and stirred till dissolved. Then 13 ml ethylene glycol (anhydrous) was added to the mixture. The resulting mixture was transferred to an autoclave and maintained at 200 °C for 2 h. The material was then washed with water and ethanol several times and dried by freeze drying. The resulting cobalt hydroxide ($Co(OH)_2$) was converted to Co_3O_4 by heat treatment in air at 350 °C for 2 h.

Synthesis of graphene. Monolayer graphene was synthesized on copper foil by CVD method. The electropolished copper foil was inserted into a quartz tube, which was then heated to 1000 °C in 20 min. After annealing for 20 min, 3.5 sccm CH_4 was inserted into the tube within 6 min. The copper foil was pulled out immediately after CH_4 was turned off. H_2/Ar (15% H_2) was used as carrier gas and a mechanical pump was used to keep the pressure in quartz tube at 1 Torr during the entire process.

Working electrode preparation. Co_3O_4 nanosheets were dispersed in a mixture of de-ionized water and isopropanol (1:1 wt ration) by a short sonication. The mixture was then centrifuged at 3000 rpm and the supernatant was centrifuged two more times. This resulted in a dilute dispersion of Co_3O_4 nanosheets which was used for electrode preparation. 16 nm Ti was thermally evaporated on the surface SiO_2 coated Si wafer. A copper strip was connected to the top of substrate using silver epoxy. Co_3O_4 nanosheets were deposited on this substrate by electrophoretic deposition (EPD) at a constant potential of 0.7 V for 6 h. For this, the substrate along with a carbon paper counter electrode was dipped in the above dispersion while the distance between them was kept the same (at 1 cm) along the deposition and also for different deposition rounds. After EPD the Cu contact was removed from the substrate and then dried at 100 °C for 1 h and then cut into two pieces. One piece was used directly as Co_3O_4 electrode. To prepare G/Co_3O_4, a graphene layer was transferred to the other part of the substrate. Graphene was transferred with a PMMA assisted method for which, a layer of poly (methyl methacrylate) (PMMA) was spin-coated onto the graphene covered copper foil. Iron chloride ($FeCl_3$) solution was then used to etch away copper. The resulted PMMA/graphene was washed by deionized water and scooped up onto the target substrate. When PMMA/graphene was dried completely, the PMMA layer was removed by acetone and isopropanol. For graphene electrode, graphene was transferred on a Ti coated Si/SiO_2 wafer with the same method. In the case of bi-G/Co_3O_4, a second graphene layer was transferred on top of G/Co_3O_4 at this step. A copper strip was attached to Ti layer for Co_3O_4 electrode and to graphene layer for G/Co_3O_4, bi-G/Co_3O_4 and graphene working electrodes. A homogeneous region of electrode surface was marked under microscope and then the contacts and edges of the marked areas were covered with epoxy resin. 1 μl of nafion (0.05 wt%) was dropped on top the exposed window and let dry at room temperature. A Pt wire and an Ag/AgCl (1 M KCl) were employed as the counter and reference electrodes, respectively. To convert the Ag/AgCl electrode potential ($E_{Ag/AgCl}$) to reversible hydrogen electrode (E_{RHE}), the following equation was used:

$$E_{RHE} = E_{Ag/AgCl} + 0.222\ V + 0.059\ pH$$

The pH of 1 ml 0.1 M KOH aqueous electrolyte was 13.

2.2. DFT calculation

Density functional theory [14] and Van der Waals approach [15] were employed in this work based on the Perdew–Burke–Ernzerhof (PBE) generalized gradient approximation [16] with interactions between ion cores and valence electrons described by the projector augmented wave (PAW) method [17] as implemented in the VASP [18] package. A plane wave basis set with a cut-off energy of 450 eV was used. Considering the strong correlation effects in transition metals, electronic structure calculations and structural relaxations were performed using a spin-dependent GGA plus Hubbard U (GGA + U, U = 2.0 eV) method [19]. A 6 × 6 supercell is used to examine the free energy changes of OER on graphene. The supercells containing excess electrons were compensated with a uniform background charge.

Computational modelling. In alkaline environment, we consider a four electron reaction paths for OER on graphene,

$$H_2O\ (l) + * \rightarrow OH^* + (H^+ + e^-) \quad (S1)$$

$$OH^* \rightarrow O^* + (H^+ + e^-) \quad (S2)$$

$$O^* + H_2O\ (l) \rightarrow OOH^* + (H^+ + e^-) \quad (S3)$$

$$OOH^* \rightarrow * + O_2\ (g) + (H^+ + e^-) \quad (S4)$$

where * stands for an active site on graphene surface, (l) and (g) refer to liquid and gas phases, respectively, and O*, OH*, and OOH* are the adsorbed intermediate.

In order to obtain the rate limiting step of OER on different sites, we calculated the adsorption Gibbs free energies of O*, OH*, and OOH* as following,

$$\Delta G_{OH^*} = E(OH^*) - E(*) - (E_{H2O} - 1/2E_{H2}) + \Delta ZPE - T\Delta S \quad (S5)$$

$$\Delta G_{O^*} = E(O^*) - E(*) - (E_{H2O} - E_{H2}) + \Delta ZPE - T\Delta S \quad (S6)$$

$$\Delta G_{OOH^*} = E(OOH^*) - E(*) - (2E_{H2O} - 3/2E_{H2}) + \Delta ZPE - T\Delta S \quad (S7)$$

Where $E(*)$, $E(O^*)$, $E(OH^*)$, and $E(OOH^*)$ are the ground state energies of a clean surface and surfaces adsorbed with O*, OH*, and OOH*, respectively. E_{H_2O} and E_{H_2} are the energies of H_2O and H_2 melecules in the gas phase. ΔZPE and $T\Delta S$ are the zero point energy and entropy corrections, which are directly taken from Ref. [24].

For each reaction step (S1) – (S4), the reaction free energy ΔG is defined as the difference between free energies of the initial and final states and is given by the expression

$$\Delta G = \Delta E + \Delta ZPE - T\Delta S - eU + k_b T \ln H^+ \quad \text{(S8)}$$

Where ΔE, e, U and $k_b T \ln H^+$ are the reaction energy difference of reactant and product molecules adsorbed on graphene surface, the charge transferred, the applied potential and the correction of the H^+ free energy by the concentration dependence of the entropy. An ideal catalyst should be able to facilitate the OER above equilibrium potential with zero overpotential which requires all the four charge transfer steps have the same free energy changes at zero potential. However, since the binding energies of the intermediate states on real catalyst surface are correlated, the ideal case cannot be achieved, and an overpotential η^{OER} is required to enable the OER; The lower the overpotential, the better the catalyst. The OER overpotential can be determined as

$$G^{\mathrm{OER}} = \max(\Delta G_1, \Delta G_2, \Delta G_3, \Delta G_4) \quad \text{(S9)}$$

$$\eta^{\mathrm{OER}} = G^{\mathrm{OER}}/e - 1.23\,\mathrm{V} \quad \text{(S10)}$$

Where, ΔG_1, ΔG_2, ΔG_3, ΔG_4 are the free energy of reaction (S1) – (S4), respectively.

Since the bindings of OH* and OOH* are related to each other, showing a constraint as for metal oxides

$$\Delta G_2^0 + \Delta G_3^0 = \Delta G_{OOH^\cdot} - \Delta G_{OH^\cdot} = 3.2\,eV \quad \text{(S11)}$$

the lower limit of overpotential is set to

$$\Delta \eta_{limit}^{OER} = \frac{\Delta G_2^0 + \Delta G_3^0}{2} - 1.23 = 0.37\,V \quad \text{(S12)}$$

3. Results and discussion

The working electrode for our model system was prepared in such a way that the electrochemical active material was fully covered with an interfacial monolayer graphene. Co_3O_4 was chosen for our system due its known electrochemical activity and also the fact that it could be grown in the form of large and thin nanosheets and more importantly isolated from any support (will be discussed in detail later). Hydrothermally synthesized Co_3O_4 nanosheets were then easily separated from growth solution and deposited on a Ti coated Si/SiO_2 substrate by EPD. Next, a CVD grown monolayer graphene (Raman spectrum is shown in Fig. S1) was transferred on top of the substrate with a PMMA assisted method. The optical image of the substrate in Fig. 1a is showing a well coverage of the substrate by graphene over a large area while Co_3O_4 nanosheets are recognizable as small dark dots spreading all over substrate underneath of graphene. To confirm the presesence of graphene on the substrate and full coverage of Co_3O_4 nanosheets, we performed point Raman analysis on different spots as well as Raman mapping of the substrate. Raman spectra of the Co_3O_4 and graphene-coated Co_3O_4 substrates are shown in Fig. S2 with assigned vibrational modes related to Co_3O_4 and graphene [20–22]. The Raman mapping was done with respect to the strongest vibrational mode of Co_3O_4 (F_{2g}) and G band of graphene (see Fig. S3). By comparing the Raman maps and the optical image of the mapped area, it can be clearly seen that while F_{2g} is only recognizable at particular regions on the substrate, G band signal is homogenously recorded from all the area. The working electrode preparation was finalized by connecting Cu stripe to graphene and creating a small exposing window for electrochemical testing by covering the graphene edges and electrical contact with epoxy resin as shown in Fig. 1b and Fig. S4. This electrode is referred as G/Co_3O_4 and for comparison, an un-covered Co_3O_4 (Co_3O_4) and graphene electrode (G) were prepared similarly (see experimental section for details).

The working electrodes were tested in a three electrode electrochemical cell. The linear sweep voltammetry (LSV) curves of the prepared electrodes in alkaline medium (0.1 M KOH) for positive potentials are shown in Fig. 2a. While graphene itself showed minor electrochemical activity, its activity is boosted once placed on top of Co_3O_4 nanosheets. G/Co_3O_4 shows similar electrochemical performance to Co_3O_4 electrode pointing towards the transference of the electrochemical activity from Co_3O_4 to graphene. A small difference between the curves is observed at higher potentials which can be due to higher rate of charge transfer to the current collector for G/Co_3O_4; While Cu contact was attached to graphene layer in G/Co_3O_4 electrode, it was connected to Ti layer in Co_3O_4 electrode and such a difference is expected. As an additional twist, we also investigated the electrochemical activity of a second layer graphene covering Co_3O_4 nanosheets. For that, another monolayer graphene was transferred on top of G/Co_3O_4 (bi-G/Co_3O_4). As can be seen in Fig. 2a, by transferring a second layer of graphene, the electrochemical activity fades significantly and reaches to the performance of the stand-alone graphene.

It is predictable that the electronic properties of graphene will be modified due to the interaction with Co_3O_4 nanosheets. To visualize the interaction of the graphene layer and Co_3O_4 nanosheets, Raman mapping was done on G/Co_3O_4 substrate with respect to the D, G and 2D bands of graphene (see Fig. S5). While D band (Fig. S5b) and G band (Fig. S3c) are almost unaffected at the contact points by Co_3O_4 and have the highest intensity at the reported wavenumbers for monolayer graphene [23,24], the 2D signal does not appear at its original wavenumber when compared with the Raman spectrum of the graphene itself (Fig. S1). In the Raman map with respect to 2672 cm^{-1}, the signal was pretty much

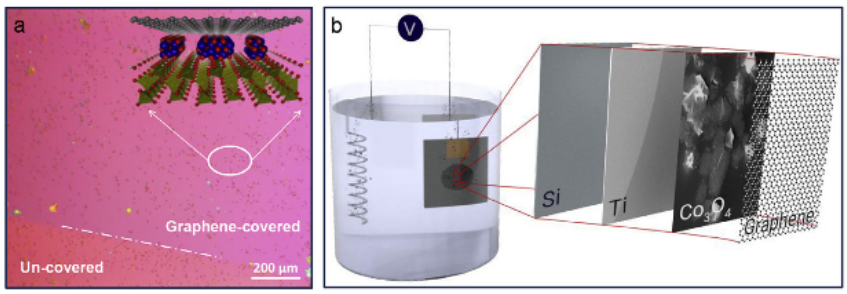

Fig. 1. a) Optical image of G/Co_3O_4 substrate over an area of ~ 1 mm^2, Co_3O_4 nanosheets are seen as dark spots all over the substrate, graphene is transferred to top part of the substrate and a dotted line distinguishes the border between graphene covered and un-covered parts of the substrate, inset: schematic illustration of the geometry of the substrate showing Co_3O_4 nanosheets (cobalt and oxygen atoms are shown as blue and red spheres) on Si/SiO_2 substrate which are fully covered with a monolayer graphene (carbon atoms as grey spheres) and b) Schematic illustration of the layer assembly of the working electrode in an electrochemical cell. (A colour version of this figure can be viewed online.)

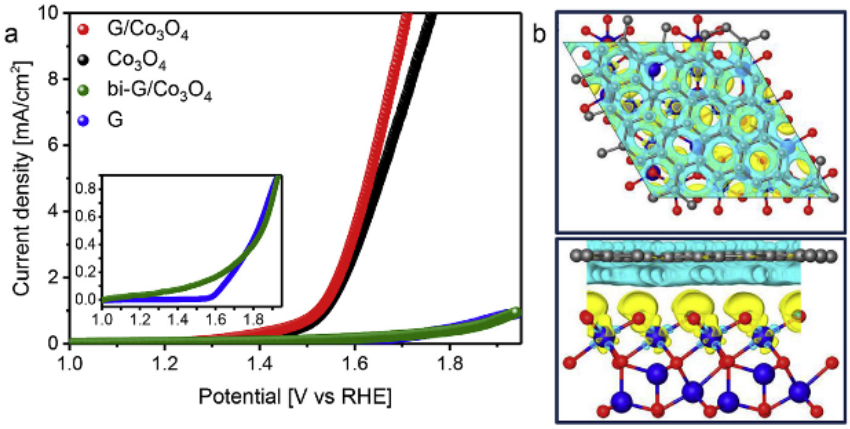

Fig. 2. a) Linear sweep voltagrams in 0.1 m KOH aqueous solution for G/Co_3O_4 (red-line), Co_3O_4 (black-line) graphene (blue-line) and bi-G/Co_3O_4 (green-line) working electrodes which shows similar electrochemical performance of G/Co_3O_4 and Co_3O_4 working electrodes that is significantly improved compare to the stand-alone graphene electrode. Inset shows a zoom-in comparison between LSV curves of graphene and bi-G/Co_3O_4 working electrodes. The scan rate was 5 mV s^{-1}, b) Computed top and side views of charge distribution of G/Co_3O_4 at isosurface of 0.001 eÅ^3. Yellow (blue) indicates electron accumulation (depletion). (A colour version of this figure can be viewed online.)

recorded with the same strength from the whole area except those regions that are in contact with under-layer Co_3O_4 and hence those regions appear as dark spots pointing towards the fact that the 2D band has shifted. By investigating the map with respect to different wavenumbers, a down-shifted by $\sim 6\ cm^{-1}$ was realized as can be seen in Fig. S5d; the contact regions appear brighter compare to the only graphene regions in the map with respect to $2666\ cm^{-1}$. The 2D signal shift has been observed in graphene-based Van der Waals heterostructures which is reported to be due to the coupling of the graphene with the under-layer material and the nature of charge transfer [25,26]. To understand the effects of the interaction, DFT calculations were employed to determine the electronic properties of G/Co_3O_4. We chose Co_3O_4 (111) surface as our model system for two reasons: (1) among all the low index facets, Co_3O_4 (111) has the lowest surface energy; (2) a relative small supercell ($\sqrt{21} \times \sqrt{21}$ of graphene on 2×2 Co_3O_4 (111)) is large enough to maintain the lattice mismatch between graphene and Co_3O_4 (111) within 1%, which minimizes the computing requirements. The optimized geometry of Co_3O_4 and G/Co_3O_4 is shown in Fig. S6. The adsorption energy of graphene on Co_3O_4 (111) is calculated to be 0.032 eV/Å^2, which is slightly higher than the reported adhesion between graphene and Cu (111) ~ 0.022 eV/Å^2 [27]. From the corresponding spatial charge density difference of G/Co_3O_4 (Fig. 2b), we observe an almost uniform charge transfer (in the form of electron donation) from graphene to Co_3O_4 that agrees well with the observed Raman shift. As a result, the Dirac point of the unfolded graphene band structure also shifts up from the Fermi level (Fig. S7). Further analysis shows that 0.027 e/atom, equivalent to 1.029×10^{14} e/cm^2, has been transferred from C to surface O atoms and hence the whole graphene sheet can be viewed as p-doped layer (positively charged) similar to nitrogen-doped graphene (Fig. S8) [28], except for the smaller charging level. Therefore, G/Co_3O_4 has the potential to show electrochemical activity as nitrogen-doped graphene does. Moreover, since the charge is distributed uniformly in G/Co_3O_4, all the C atoms could act similarly as active sites during electrocatalytic reactions.

The electrochemical reaction that we specifically looked at was OER which is one of the half reactions of the water splitting reaction occurring on the surface of anode. As the surface adsorption of hydroxide ions (OH^-) is the first step of the 4-step OER reaction in alkaline electrolyte and there is no possibility for OH^- ions to intercalate graphene, the electrocatalytic performance of graphene covering the main catalyst can be verified in this system without any ambiguity. This system is different from the often reported electrocatalysis of the coated catalyst nanoparticles with carbon layers where in most cases an improvement in activity compared to the catalyst itself is reported [29–39]. However in many of these studies, since the main concern is the catalytic performance of the whole system rather than the actual contribution of each element, not much attention is given to the real active surface. In contrast in construction of our system, the main target was to build the working electrode in such a way that the current is only collected from the surface of graphene (which is the electrochemically inactive element of the system and is in direct contact with the electrolyte). In this way any collected signal was originating from the presence of the under-layer material. To be successful in our demonstration, any factor that could possibly influence the charge distribution except the under-layer material should be prohibited. These factors include the presence of guest elements, defects and curvature within the graphene layer. For example, by guest element doping of graphitic carbon, not only the charge distribution is altered but also many defects are introduced to the structure which indeed opens up a pathway for ion transfer. Nitrogen doping can turn the catalytically inactive graphene and carbon nanotubes to a competing best metal free catalyst material for oxygen reduction reaction [40]. Hence, dissimilar to our construction, the catalytic performance of the encapsulated metal nanoparticles within the doped carbon shells is the synergistic contribution of both core and shell material [41,42]. In addition, due to the presence of defects, the actual electrochemical reaction can happen in the confined region between catalyst and carbon layer. In other words, ions can be transferred through the defects and channels and reach to the surface of the catalyst material for the reaction to occur. Curvature is also manipulating the charge distribution in carbon nanostructures. A down shift in Fermi level is reported in carbon nanotubes compared to graphene due to the curvature effect [43]. In our electrode design, to avoid any curvature, each element of G/Co_3O_4 working electrode needed to be positioned flatly on top of the previous layer accomplishing the maximum contact points while at the same time the risk of inducing curvature was minimized. Hence, it was required to adopt a thin and large area electrochemically active material for our system even though we were aware of inferior activity of Co_3O_4 in the form of nanosheets compared to its 3D counterpart in catalyzing OER. The choice of Co_3O_4 over other active materials for OER such as noble metal nanostructures was based on both experimental and calculation

requirements which were restricting the choice of under-layer material. Co_3O_4 is among few electrochemically active metal oxides that can be synthesized and isolated in solution in the form of thin and laterally large nanosheets which is not possible for many other electrocatalytically active nanostructures [12,44]. The second reason was the relatively simpler structure of Co_3O_4 for DFT calculation compare to the more complex mixed metal oxide catalysts with better catalytic performance. However, since the catalytic performance of the under-layere catalyst was not the main focus of the study and adopting an optimum working electrode assembly to investigate our hypothesis was the foremost concern, Co_3O_4 nanosheet was among the best candidates. Electron microscopy images of our synthesized Co_3O_4 nanosheets (Fig. S9) confirm the formation of nanosheets with a lateral size of ~ 2 μm with an average thickness of 6 nm and not more than 10 nm (see Fig. S10). The electrochemical activity of the nanosheets itself is comparable with the previous reports on Co_3O_4 [22,45–47]. Co_3O_4 nanosheets show polycrystalline structure similar to other nanostructured metal oxides which have gone through phase transformation from hydroxide to oxide phase during synthesis [48,49]. In our case, Co_3O_4 nanosheets have formed by a phase transformation from the as synthesized $Co(OH)_2$ (see XRD patterns in Fig. S11) *via* temperature treatment in air which resulted in a polycrystalline structure confirmed by high resolution transmission electron microscopy and selected area electron diffraction pattern shown in Fig. S12. As shown in Fig. S13, low voltage EPD resulted in 2–3% coverage of the substrate by Co_3O_4 nanosheets (from statistical measurement on SEM images of several substrates which were prepared with the same EPD condition) with minor chance of overlapping and hence giving rise to maximum contact points with the graphene once transferred on top. After transferring graphene on top of Co_3O_4 electrodes, they were carefully characterized before testing and those matching our desire were chosen. However, from a practical point of view, it is possible for a large area graphene to damage during transfer or when it comes to contact with liquid electrolyte. Nevertheless if the damage is in the form of a small hole, as there is a large affinity for hydroxide ions to bond to the edge-carbon, it seems unlikely for OH^- ions to penetrate under the graphene layer from the edges of the hole considering large adhesion of graphene to the substrate. DFT calculation has shown that, under common experimental condition, oxygen needs to overcome an energy barrier of 1 eV to intercalate the graphene edge on Cu(111) and higher (1.24 eV) in the case of Ni(111) [50]. Water intercalation of graphene on metal oxide substrate can occur either at high temperatures (90 °C) or at low pressures [36]. Hence, in our experimental condition, hydroxide ions most probably just block the damaged regions (if they exist) and inhibit the flow of electrolyte under graphene. From experimental point of view, since OH^- cannot tunnel through graphene, the only way for ions to reach to the surface of Co_3O_4 nanosheets is the flow of electrolyte under graphene from the edges of the damaged areas. If this happens the graphene layer would be certainly destroyed, starting from damaged regions and expanding through the whole electrode surface as the reaction continues. To confirm the stability of graphene during the electrochemical testing, we repeated the Raman mapping on the tested electrode. As shown in Figs. S15a–c, Raman mapping with respect to D and 2D band confirm that the monolayer graphene is well conserved after electrochemical testing (compare Figs. S5 and S14). Furthermore, the chronoamperometric response of the G/Co_3O_4 electrode at a constant potential of 1.66 V *vs.* RHE is shown in Fig. S14d which shows that the measured current density from the working electrode remains almost constant over 250 min of measurement after an initial attenuation.

To obtain deep insights into the mechanism of electrochemical activity of G/Co_3O_4 system, we investigated the energetics of OER on G/Co_3O_4 and compared it with pristine graphene. A four electron reaction path has been adopted to identify the fundamental aspect of OER on G/Co_3O_4. The detailed paths and the corresponding free energies of the reactions are listed in Supplementary equations S1-S10. In electrochemistry, overpotential (η^{OER}) is a measure to evaluate the activity of the electrode material to catalyze certain electrochemical reaction and is defined as the difference between the measured and the thermodynamically predicted potential for each half reactions. The calculated standard free energy diagram with lowest η^{OER} of OER sub-steps on G/Co_3O_4 is shown in Fig. 3a. On G/Co_3O_4, OH* adsorption shows the largest free energy change (ΔG_1^0) of 2.21 eV, resulting in an overpotential of 0.98 V, which is the rate-limiting step for the OER. Unlike doped graphene [28] whose catalytic activity is highly dependent on the adsorption site, OH* shows a consistent adsorption behavior on G/Co_3O_4 (Fig. S15). The corresponding η^{OER} is ranging from 0.98 to 1.13 V (Fig. 3a), suggesting a nearly homogeneous electrochemical activity on G/Co_3O_4. Compared to the OER overpotential of pristine (1.53 V) and N-doped (0.40 V) graphene (Fig. S16), G/Co_3O_4 sits in the middle due to the charge transfer induced self-charging of graphene. The optimized adsorption site of O* is on the bridge of C=C bond (Fig. S17), which is also different from doped graphene but similar to pristine graphene [51]. Moreover, bi-G/Co_3O_4 shows almost the same free energy diagram as pristine graphene since there is no charge transfer between two graphene layers (Fig. S18). This result shows that dissimilar to the curved carbon layers where charge penetration can occur through several layers [33], on fully uncurved (flat) graphene layer and in the absence of curvature effect charge transfer can only occur in monolayer graphene positioned at an optimum distance from metal(oxide) layer. These results indicate that charging or doping is essential for the OH* adsorption on graphene. On neutral graphene, OH* is hard to be adsorbed, which limits the catalytic activity of graphene. With a small amount of evenly distributed charge, OH* adsorption becomes easier on G/Co_3O_4, which enables the OER as we observed in our experiments. We also expect other O-rich Co_3O_4 surfaces, including (110) and (311), supported graphene should show similar catalytic activity due to the charge transfer between C and O atoms. With higher localized charging, OH* adsorption no longer limits the OER, but the O* → OOH* transformation does. Therefore, if improvement of the OER activity of graphene is specifically desired, using a more electronegative under-layer material which is indeed a stronger acceptor or even applying gate voltage could be considered.

We then proceed to investigate the free energy changes of OER on graphene at different charging levels varying from −0.083 to 0.111 e/atom (band structures of graphene at the highest charging level are shown in Fig. S19). As shown in Fig. S20, we find ΔG_{OH^*} and ΔG_{OOH^*} show a linear relationship with a slope of ~ 1 and an intercept of 3.148, which is close to metal oxides and doped graphene, yielding a lower overpotential limit of 0.34 V. Fig. 3b summarizes the OER free energy changes on graphene as a function of charging level. For positively charged graphene, the trend of free energy changes is clear; with increased charging level of graphene, the free energies of OH* adsorption (ΔG_1 -red line) and O* → OOH* transformation (ΔG_3 -green line) decreases at the cost of free energies increase of OH* → O* (ΔG_2 -blue line) and OOH* → O_2 transformation (ΔG_4-pink line). The fitting for the free energy changes shows very good linear scaling. At the charging level of 0.027 *e*/atom, the free energy changes of OER on pristine graphene are comparable to that of G/Co_3O_4, suggesting that charging is indeed the key factor of the observed electrochemical activity of G/Co_3O_4. Further analysis shows the overpotential decreases as ΔG_1 is reduced by charging. At charging level of 0.086 *e*/atom, ΔG_2 equals to ΔG_3 ~1.57 eV, which is close to the lower limit boundary.

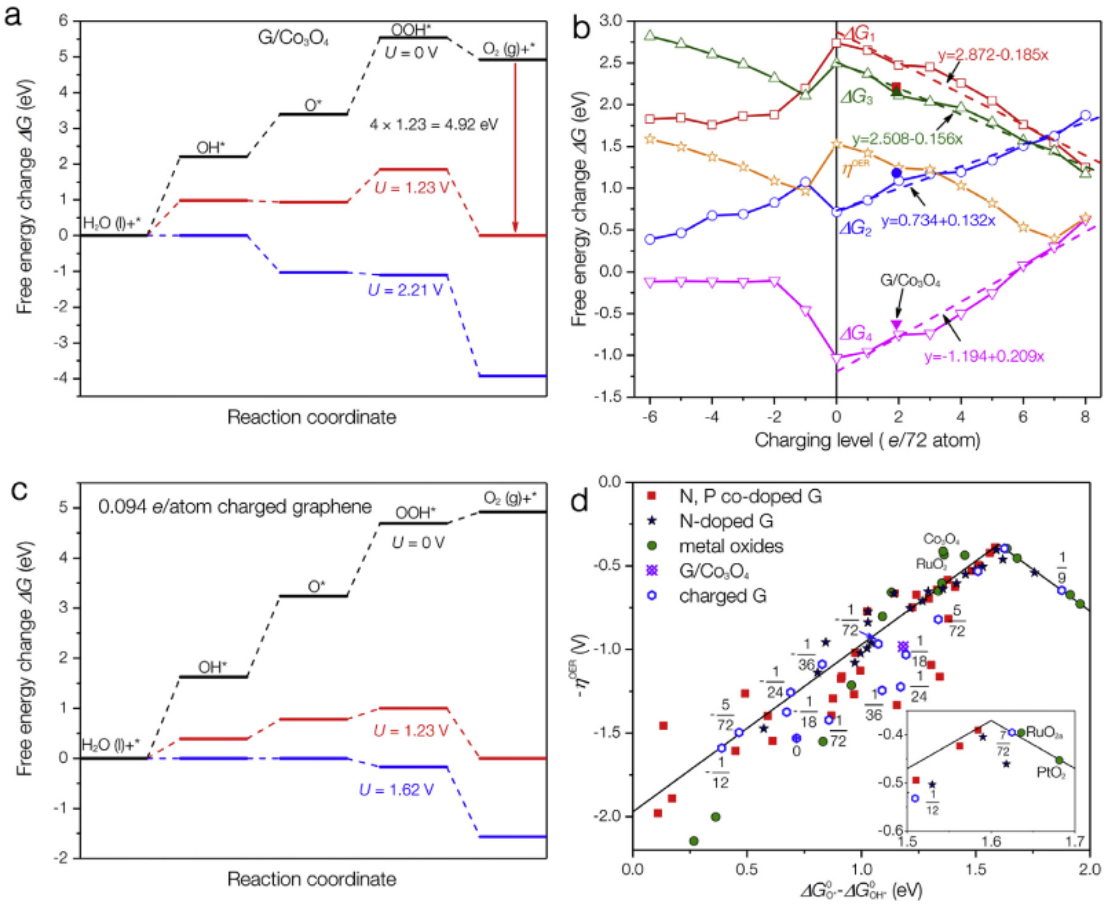

Fig. 3. a) Free energy diagrams for the OER on G/Co_3O_4 at zero potential ($U = 0$ V), equilibrium potential ($U = 1.23$ V), and at the potential where all the steps become downhill (2.21 V), b) Free energy changes of OER sub-steps and corresponding OER overpotentials on graphene at difference charging level from −0.083 to 0.111 e/atom (solid lines with open symbols). The dashed lines show the linear fitting of the free energy changes on positively charged graphene. The solid symbols show the free energy changes on G/Co_3O_4, c) Free energy diagrams for the OER on graphene at charging level 0.094 *e*/atom at zero potential ($U = 0$ V), equilibrium potential ($U = 1.23$ V), and at the potential where all the steps become downhill (1.62 V), and d) OER volcano plot of overpotential $-\eta^{OER}$ versus the adsorption energy difference between OH* and OOH* for G/Co_3O_4 and charged graphene. The theoretically predicted OER overpotentials for N-doped and N, P co-doped graphene, and metal oxides are also shown for comparison [28,52,53]. (A colour version of this figure can be viewed online.)

However, ΔG_1 is still the highest free energy change for OER sub-step at ~1.73 eV, resulting in an overpotential of 0.50 V. With a bit more charging of ~0.094 e/atom, ΔG_1 becomes the same as ΔG_3 at ~1.62 eV, which corresponds to an overpotential of 0.39 V. Free energy diagrams for the OER on graphene at charging level of 0.094 *e*/atom are shown in Fig. 3c. Further charging the graphene will increase the overpotential due to the increasing of ΔG_3. On the other hand, negative charging shows different effects. At low charging level of ~ −0.014 *e*/atom, the free energies show the same trend as positive charging. The overpotential is reduced to 0.97 V, which is even lower than the overpotential of positively charged graphene at the same level. When the charging level is increased to −0.028 e/atom, ΔG_1 and ΔG_4 still follow the same trend, but the trend of ΔG_2 and ΔG_3 is reversed, where ΔG_2 starts to decrease and ΔG_3 starts to increase. Analyzing the adsorption geometry of O* and OOH* on charged graphene, we found that the adsorption site of O* on graphene changed from the bridge site to the top site of C atom (Fig. S21), where the latter is calculated to be 0.39 eV lower than former. Thus, ΔG_2 is decreased, and ΔG_3 is increased due to the linear relationship with ΔG_2. At higher charging level, ΔG_1 and ΔG_4 become constant, and the trend of ΔG_2 and ΔG_3 remains. As a result, the overpotential increases when the charging level is greater than −0.014 *e*/atom. Overall, the minimum overpotential of charged graphene for OER is 0.39 eV, comparable to those of the best catalysts identified theoretically as shown in the volcano plot (Fig. 3d). This indicates that the graphene could outperform the electrochemical activity of most of its metal oxides and doped-graphene counterparts if charged to an optimum level. The charging level can be regulated by the choice of under-layer material.

4. Conclusion

In summary, we explored the capability of monolayer graphene (with negligible electrochemical activity) to adopt the electrochemical activity from a material which is placed in its close vicinity. We built up a model system in which Co_3O_4 nanosheets as the electrochemically active material was uniformly covered by a monolayer graphene. We then compared the electrochemical performance of this model system with un-covered Co_3O_4 during electrochemical OER. We show that graphene fully adopts the electrochemical performance of Co_3O_4 and while stand-alone graphene is fully inactive material, once placed on top of Co_3O_4 shows similar performance to Co_3O_4. We observe that the electrochemical activity is quenched completely when more than one graphene layer is placed on top of Co_3O_4. Based on DFT calculations, the

electrochemically inactive monolayer graphene turns into an active material due to electron donation from graphene to the buried Co_3O_4 which indeed transform the graphene to a positively charged surface.

Acknowledgements

T.S. and H.R.B acknowledge Swedish Research Council (Grant No. 2015-06462 and 2015-00520), XZ acknowledges Air Force Office of Scientific Research (AFOSR-Grant No. FA9550-14-1-0268). A.Z and H.R.B acknowledge support in part by the Director, Office of Science, Office of Basic Energy Sciences, Materials Sciences and Engineering Division, of the U.S. Department of Energy under Contract No. DE-AC02-05-CH11231, within the sp2-Bonded Materials Program (KC2207) which provided for complementary materials synthesis and TEM and Raman characterization, and student support; and by the National Science Foundation under Grant No. DMR-1206512 which provided for development of complementary sample lift-off and transfer methodologies. Shared equipment authority (SEA) at Rice University is acknowledged. Matt Gilbert from University of California at Berkeley is acknowledged for his contribution.

Appendix A. Supplementary data

Supplementary data to this article can be found online at https://doi.org/10.1016/j.carbon.2018.09.056.

References

[1] G.R. Bhimanapati, Z. Lin, V. Meunier, Y. Jung, J. Cha, S. Das, et al., Recent advances in two-dimensional materials beyond graphene, ACS Nano 9 (12) (2015) 11509–11539.
[2] X. Zhou, S. He, K.A. Brown, J. Mendez-Arroyo, F. Boey, C.A. Mirkin, Locally altering the electronic properties of graphene by nanoscopically doping it with rhodamine 6G, Nano Lett. 13 (4) (2013) 1616–1621.
[3] H. Md Tanvir, J.S. Brian, M. Price, R. Conor, D. Hung, G. Zygmunt, et al., Modifying optical properties of reduced/graphene oxide with controlled ozone and thermal treatment in aqueous suspensions, Nanotechnology 28 (6) (2017) 065705.
[4] T. Ma, Z. Liu, J. Wen, Y. Gao, X. Ren, H. Chen, et al., Tailoring the thermal and electrical transport properties of graphene films by grain size engineering, Nat. Commun. 8 (2017) 14486.
[5] C.N.R. Rao, R. Voggu, Charge-transfer with graphene and nanotubes, Mater. Today 13 (9) (2010) 34–40.
[6] A.T. Sergey Kopylov, Sergey Kubatkin, Vladimir I. Fal'ko, Charge transfer between epitaxial graphene and silicon carbide, Appl. Phys. Lett. 97 (11) (2010).
[7] A. Matković, M. Kratzer, B. Kaufmann, J. Vujin, R. Gajić, C. Teichert, Probing charge transfer between molecular semiconductors and graphene, Sci. Rep. 7 (1) (2017) 9544.
[8] Y. Cao, V. Fatemi, S. Fang, K. Watanabe, T. Taniguchi, E. Kaxiras, et al., Unconventional superconductivity in magic-angle graphene superlattices, Nature (2018) 43–50.
[9] H. Tetlow, J. Posthuma de Boer, I.J. Ford, D.D. Vvedensky, J. Coraux, L. Kantorovich, Growth of epitaxial graphene: theory and experiment, Phys. Rep. 542 (3) (2014) 195–295.
[10] K.S. Novoselov, A.K. Geim, S.V. Morozov, D. Jiang, Y. Zhang, S.V. Dubonos, et al., Electric field effect in atomically thin carbon films, Science 306 (5696) (2004) 666.
[11] D.A.C. Brownson, S.A. Varey, F. Hussain, S.J. Haigh, C.E. Banks, Electrochemical properties of CVD grown pristine graphene: monolayer- vs. quasi-graphene, Nanoscale 6 (3) (2014) 1607–1621.
[12] N.-T. Suen, S.-F. Hung, Q. Quan, N. Zhang, Y.-J. Xu, H.M. Chen, Electrocatalysis for the oxygen evolution reaction: recent development and future perspectives, Chem. Soc. Rev. 46 (2) (2017) 337–365.
[13] Z. Sun, T. Liao, Y. Dou, S.M. Hwang, M.-S. Park, L. Jiang, et al., Generalized Self-assembly of Scalable Two-dimensional Transition Metal Oxide Nanosheets 5, 2014, p. 3813.
[14] J. Harl, L. Schimka, G. Kresse, Assessing the quality of the random phase approximation for lattice constants and atomization energies of solids, Phys. Rev. B 81 (11) (2010) 115126.
[15] A. Tkatchenko, M. Scheffler, Accurate molecular van der waals interactions from ground-state electron density and free-atom reference data, Phys. Rev. Lett. 102 (7) (2009) 073005.
[16] J.P. Perdew, K. Burke, M. Ernzerhof, Generalized gradient approximation made simple, Phys. Rev. Lett. 77 (18) (1996) 3865–3868.
[17] P.E. Blöchl, Projector augmented-wave method, Phys. Rev. B 50 (24) (1994) 17953–17979.
[18] G. Kresse, J. Furthmüller, Efficient iterative schemes for ab initio total-energy calculations using a plane-wave basis set, Phys. Rev. B 54 (16) (1996) 11169–11186.
[19] J. Zhu, X. Ren, J. Liu, W. Zhang, Z. Wen, Unraveling the catalytic mechanism of Co3O4 for the oxygen evolution reaction in a Li–O2 battery, ACS Catal. 5 (1) (2015) 73–81.
[20] V.G. Hadjiev, M.N. Iliev, I.V. Vergilov, The Raman spectra of Co 3 O 4, J. Phys. C Solid State Phys. 21 (7) (1988) L199.
[21] B. Rivas-Murias, V. Salgueiriño, Thermodynamic CoO–Co3O4 crossover using Raman spectroscopy in magnetic octahedron-shaped nanocrystals, J. Raman Spectrosc. 48 (6) (2017) 837–841.
[22] T. Sharifi, E. Gracia-Espino, X. Jia, R. Sandström, T. Wågberg, Comprehensive study of an earth-abundant bifunctional 3D electrode for efficient water electrolysis in alkaline medium, ACS Appl. Mater. Interfaces 7 (51) (2015) 28148–28155.
[23] Y.y. Wang, Z.h. Ni, T. Yu, Z.X. Shen, H.m. Wang, Y.h. Wu, et al., Raman studies of monolayer graphene: the substrate effect, J. Phys. Chem. C 112 (29) (2008) 10637–10640.
[24] A.C. Ferrari, J.C. Meyer, V. Scardaci, C. Casiraghi, M. Lazzeri, F. Mauri, et al., Raman spectrum of graphene and graphene layers, Phys. Rev. Lett. 97 (18) (2006) 187401.
[25] D. Pierucci, H. Henck, C.H. Naylor, H. Sediri, E. Lhuillier, A. Balan, et al., Large area molybdenum disulphide- epitaxial graphene vertical Van der Waals heterostructures 6, 2016, p. 26656.
[26] Z. Ben Aziza, H. Henck, D. Pierucci, M.G. Silly, E. Lhuillier, G. Patriarche, et al., van der Waals epitaxy of GaSe/graphene heterostructure: electronic and interfacial properties, ACS Nano 10 (10) (2016) 9679–9686.
[27] T. Yoon, W.C. Shin, T.Y. Kim, J.H. Mun, T.-S. Kim, B.J. Cho, Direct measurement of adhesion energy of monolayer graphene as-grown on copper and its application to renewable transfer process, Nano Lett. 12 (3) (2012) 1448–1452.
[28] M. Li, L. Zhang, Q. Xu, J. Niu, Z. Xia, N-doped graphene as catalysts for oxygen reduction and oxygen evolution reactions: theoretical considerations, J. Catal. 314 (2014) 66–72.
[29] J. Deng, P. Ren, D. Deng, L. Yu, F. Yang, X. Bao, Highly active and durable non-precious-metal catalysts encapsulated in carbon nanotubes for hydrogen evolution reaction, Energy Environ. Sci. 7 (6) (2014) 1919–1923.
[30] X. Zou, X. Huang, A. Goswami, R. Silva, B.R. Sathe, E. Mikmeková, et al., Cobalt-embedded nitrogen-rich carbon nanotubes efficiently catalyze hydrogen evolution reaction at all pH values, Angew. Chem. Int. Ed. 53 (17) (2014) 4372–4376.
[31] L. Gao, Q. Fu, M. Wei, Y. Zhu, Q. Liu, E. Crumlin, et al., Enhanced nickel-catalyzed methanation confined under hexagonal boron nitride shells, ACS Catal. 6 (10) (2016) 6814–6822.
[32] L. Gao, Y. Wang, H. Li, Q. Li, N. Ta, L. Zhuang, et al., A nickel nanocatalyst within a h-BN shell for enhanced hydrogen oxidation reactions, Chem. Sci. 8 (8) (2017) 5728–5734.
[33] J. Deng, P. Ren, D. Deng, X. Bao, Enhanced electron penetration through an ultrathin graphene layer for highly efficient catalysis of the hydrogen evolution reaction, Angew. Chem. Int. Ed. 54 (7) (2015) 2100–2104.
[34] X. Cui, P. Ren, D. Deng, J. Deng, X. Bao, Single layer graphene encapsulating non-precious metals as high-performance electrocatalysts for water oxidation, Energy Environ. Sci. 9 (1) (2016) 123–129.
[35] M. Sun, Q. Fu, L. Gao, Y. Zheng, Y. Li, M. Chen, et al., Catalysis under shell: improved CO oxidation reaction confined in Pt@h-BN core–shell nanoreactors, Nano Res. 10 (4) (2017) 1403–1412.
[36] Q. Fu, X. Bao, Surface chemistry and catalysis confined under two-dimensional materials, Chem. Soc. Rev. 46 (7) (2017) 1842–1874.
[37] L. Ferrighi, M. Datteo, G. Fazio, C. Di Valentin, Catalysis under cover: enhanced reactivity at the interface between (doped) graphene and anatase TiO2, J. Am. Chem. Soc. 138 (23) (2016) 7365–7376.
[38] D. Deng, K.S. Novoselov, Q. Fu, N. Zheng, Z. Tian, X. Bao, Catalysis with two-dimensional materials and their heterostructures, Nat. Nanotechnol. 11 (3) (2016) 218–230.
[39] D. Deng, L. Yu, X. Chen, G. Wang, L. Jin, X. Pan, et al., Iron encapsulated within pod-like carbon nanotubes for oxygen reduction reaction, Angew. Chem. Int. Ed. 52 (1) (2013) 371–375.
[40] T. Sharifi, G. Hu, X. Jia, T. Wågberg, formation of active sites for oxygen reduction reactions by transformation of nitrogen functionalities in nitrogen-doped carbon nanotubes, ACS Nano 6 (10) (2012) 8904–8912.
[41] W. Zhou, J. Zhou, Y. Zhou, J. Lu, K. Zhou, L. Yang, et al., N-doped carbon-wrapped cobalt nanoparticles on N-doped graphene nanosheets for high-efficiency hydrogen production, Chem. Mater. 27 (6) (2015) 2026–2032.
[42] W. Min-Qiang, Y. Cui, L. Heng, X. Maowen, B. Shu-Juan, Nanosized metal phosphides embedded in nitrogen-doped porous carbon nanofibers for enhanced hydrogen evolution at all pH values, Angew. Chem. Int. Ed. 57 (7) (2018) 1963–1967.
[43] W.S. Su, T.C. Leung, C.T. Chan, Work function of single-walled and multiwalled carbon nanotubes: first-principles study, Phys. Rev. B 76 (23) (2007) 235413.
[44] T. Reier, M. Oezaslan, P. Strasser, Electrocatalytic oxygen evolution reaction (OER) on Ru, Ir, and Pt catalysts: a comparative study of nanoparticles and bulk materials, ACS Catal. 2 (8) (2012) 1765–1772.

[45] T.N. Pham, T. Sharifi, R. Sandström, W. Siljebo, A. Shchukarev, K. Kordas, et al., Robust hierarchical 3D carbon foam electrode for efficient water electrolysis, Sci. Rep. 7 (1) (2017) 6112.
[46] Q. He, Q. Li, S. Khene, X. Ren, F.E. López-Suárez, D. Lozano-Castelló, et al., High-loading cobalt oxide coupled with nitrogen-doped graphene for oxygen reduction in anion-exchange-membrane alkaline fuel cells, J. Phys. Chem. C 117 (17) (2013) 8697–8707.
[47] T. Zhang, C. He, F. Sun, Y. Ding, M. Wang, L. Peng, et al., Co3O4 Nanoparticles Anchored on Nitrogen-doped Reduced Graphene Oxide as a Multifunctional Catalyst for H2O2 Reduction, Oxygen Reduction and Evolution Reaction 7, 2017, p. 43638.
[48] X. Zhao, F. Zhang, S. Xu, D.G. Evans, X. Duan, From layered double hydroxides to ZnO-based mixed metal oxides by thermal decomposition: transformation mechanism and UV-blocking properties of the product, Chem. Mater. 22 (13) (2010) 3933–3942.
[49] T. Takei, H. Fuse, A. Miura, N. Kumada, Topotactic transformation of Ni-based layered double hydroxide film to layered metal oxide and hydroxide, Appl. Clay Sci. 124 (Supplement C) (2016) 236–242.
[50] L. Ma, X.C. Zeng, J. Wang, Oxygen intercalation of graphene on transition metal substrate: an edge-limited mechanism, J. Phys. Chem. Lett. 6 (20) (2015) 4099–4105.
[51] X. Kong, Q. Liu, D. Chen, G. Chen, Identifying the active sites on N-doped graphene toward oxygen evolution reaction, ChemCatChem 9 (5) (2017) 846–852.
[52] J. Zhang, Z. Zhao, Z. Xia, L. Dai, A metal-free bifunctional electrocatalyst for oxygen reduction and oxygen evolution reactions, Nat. Nanotechnol. 10 (5) (2015) 444–452.
[53] I.C. Man, H.-Y. Su, F. Calle-Vallejo, H.A. Hansen, J.I. Martínez, N.G. Inoglu, et al., Universality in oxygen evolution electrocatalysis on oxide surfaces, ChemCatChem 3 (7) (2011) 1159–1165.